Engineering Fracture Mechanics 77 (2010) 348–358

Contents lists available at ScienceDirect

Engineering Fracture Mechanics

journal homepage: www.elsevier.com/locate/engfracmech

An asymptotic matching approach to shallow-notched structural elements

Pietro Cornetti [a,*], David Taylor [b], Alberto Carpinteri [a]

[a] Department of Structural Engineering and Geotechnics, Politecnico di Torino, Turin, Italy
[b] Department of Mechanical and Manufactural Engineering, Trinity College, Dublin, Ireland

ARTICLE INFO

Article history:
Received 6 March 2009
Accepted 28 April 2009
Available online 6 May 2009

Keywords:
Shallow notches
V-notches
Multiscale analysis
Asymptotic matching
Brittleness number
Finite fracture mechanics

ABSTRACT

Fracture in brittle material specimens with V-notches is satisfactorily described assuming as governing parameter the generalized (or notch) stress intensity factor, whose anomalous physical dimensions depend on the notch opening angle. Its critical value, i.e. the generalized toughness, can then be linked to the material strength and toughness according to a number of fracture criteria available in the literature. However, all these criteria provide an infinite failure load as the notch depth tends to zero, this undesirable property being shared with Linear Elastic Fracture Mechanics when applied to vanishing cracks. Aim of the present paper is to overcome this shortcoming. The analysis of the notched specimens is carried out by means of a multiscale approach according to which the problem is solved separately in the region far away from the notch (the outer field) and in the region close to the notch (the inner field). Hence, the asymptotic matching technique can be exploited to achieve the overall solution. Although the procedure is general, i.e. it may be applied to any notch shape, numerical computations refer to sharp V-notches with a re-entrant corner equal to 120°. Comparison with experimental data obtained by testing polystyrene specimens turns out to be more than satisfactory.

1. Introduction

The problem of a linear elastic plate containing a re-entrant corner (of amplitude ω) was addressed by Williams in his pioneering work [26]. Restricting the analysis to mode *I* loading, his solution shows that the stresses at the vertex of the angular corner are unbounded. The stress singularity is of order $1-\lambda$, where $\lambda(\omega)$ is the solution of the transcendental equation derived by Williams [26] and is comprised between 1/2 ($\omega = 0°$) and 1 ($\omega = 180°$). Hence:

$$\sigma_x(y) = K_I^* \Big/ (2\pi y)^{1-\lambda} \tag{1}$$

where y is the V-notch bisector and σ_x is the normal stress directed along x (see Fig. 1a). K_I^* is the generalized SIF (sometimes referred to as notch-SIF), whose value depends on geometry and loading far from the notch. Its physical dimensions vary along with ω from those of a SIF ($\omega = 0°$) to those of a stress ($\omega = 180°$). In Sections 5 and 6 the case $\omega = 120°$ will be considered in detail, for which $\lambda = 0.6157$.

Since, at the vertex, the stress is singular and, at the same time, with a singularity of order less than ½, both strength criteria and Linear Elastic Fracture Mechanics (LEFM) fail in predicting failure of specimens containing re-entrant corners. In analogy with LEFM, one may assume the generalized SIF to be the parameter governing failure [2], i.e.:

$$K_I^* = K_{Ic}^* \tag{2}$$

* Corresponding author. Tel.: +39 0115644901; fax: +39 0115644899.
E-mail addresses: pietro.cornetti@polito.it (P. Cornetti), dtaylor@tcd.ie (D. Taylor), alberto.carpinteri@polito.it (A. Carpinteri).

0013-7944/$ - see front matter © 2009 Elsevier Ltd. All rights reserved.
doi:10.1016/j.engfracmech.2009.04.013

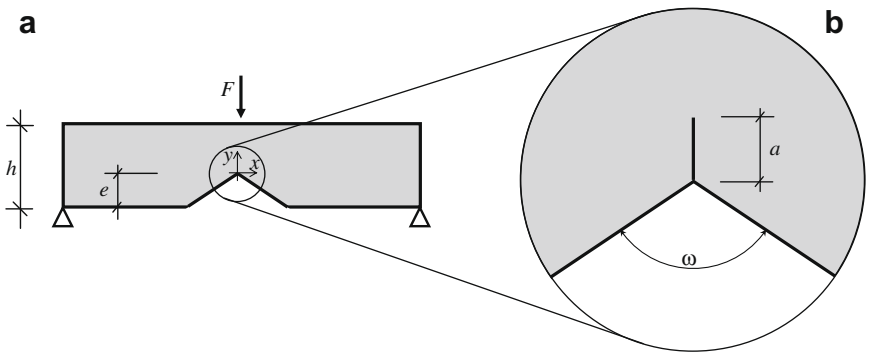

Fig. 1. Specimen with a full-sized V-notch subjected to mode *I* loading (a) and detail of the notch vertex if a short crack $a \ll e, h$ is present at the tip (b).

where K_{Ic}^{*} is named generalized fracture toughness. Carpinteri himself [2], by testing V-notched PMMA specimens, checked successfully the soundness of the criterion (2).

Later, researchers tried to provide a mechanical explanation to Eq. (2) by relating the generalized fracture toughness to the tensile strength and the fracture toughness of the tested material according to different assumptions. However, all of them (e.g. [5,7,14,15,21,22]) may be cast into the following expression:

$$K_{\mathrm{Ic}}^{*} = \xi(\omega)\frac{K_{\mathrm{Ic}}^{2(1-\lambda)}}{\sigma_{\mathrm{u}}^{1-2\lambda}} \tag{3}$$

where $\xi(\omega)$ is a dimensionless coefficient depending on the notch opening angle and on the criterion adopted. Note that, in every approach, $\xi(\omega)$ is equal to one for $\omega = 0^{\circ}$ ($\lambda = 1/2$) and $\omega = 180^{\circ}$ ($\lambda = 1$), so that the classical LEFM failure criterion $K_{\mathrm{I}} = K_{\mathrm{Ic}}$ and strength criterion $\sigma_{\max} = \sigma_{\mathrm{u}}$ are easily recovered from Eq. (2) in the extreme cases.

Although quite general, the failure criterion (2) shows for V-notches the same drawback that LEFM shows for cracks: it provides infinite failure loads as the notch depth tends to vanish. In other words, for shallow V-notches, predictions provided by Eq. (2) are inaccurate since they tend to overestimate the actual failure load. Aim of the present paper is to analyse in details the problem of shallow notches. This problem will be addressed, from a physical point of view, by means of the Finite Fracture Mechanics (FFM) and, from a mathematical point of view, by exploiting the asymptotic matching technique.

The plan of the paper is as follows. In Section 2, the bases of FFM are outlined and applied to the problem of specimen containing full-sized V-notches. In Section 3, the asymptotic analysis of a shallow-notched specimen is carried out, independently of the notch shape. In Section 4, a path-independent integral is exploited to compute the strain energy release caused by a discrete crack propagation. In Section 5, the failure criterion is finally achieved and numerically provided when the shallow notch is a re-entrant corner with the opening angle of 120°. Finally, in Section 6 a comparison with experimental data obtained by testing polystyrene specimens is performed, showing an excellent agreement between theory and experiments.

Before starting with the analysis of shallow-notched components, we want to mention that the asymptotic matching technique has been exploited also to analyse the influence of the notch root radius and of mixed mode loading on failure of (full-sized) V-notched specimens [16,27]. Eventually, note that, from a numerical point of view, crack initiation at stress concentrations is usually addressed by means of the cohesive crack model [3,4,11]. However, a direct numerical implementation of FFM is also possible as recently provided by Hebel and Becker [13].

2. Finite fracture mechanics and V-notches

Let us now consider (Fig. 1a) the problem of a specimen with a full-sized V-notch (as opposed to a shallow V-notch). It is well-known that classical strength criteria as well as LEFM fail in predicting the strength of V-notched components, being singular the stress field and null the stress intensity factor. In this section, briefly recalling the results obtained in [5], it will be shown that FFM is able to predict a finite strength for specimens with re-entrant corners and, at the same time, it provides a physical meaning to the heuristic criterion (2).

Different versions of the FFM exist. The simplest one assumes that cracks grow by a finite crack extension Δa, i.e. Δa is a material characteristic length [20,25]. However, more sophisticated versions of FFM have been proposed coupling energy balance and stress requirements for crack advancement [8,15]. We will follow the approach proposed in [8], hereafter denoted as coupled FFM.

Accordingly, the energy balance implies that a crack of length Δa may occur only if the strain energy release rate G is higher than the fracture energy G_{F}. With respect to classical LEFM, the differentials are replaced by finite differences:

$$G = \frac{\Delta \Phi}{\Delta a} \geqslant G_{\mathrm{F}} \tag{4}$$

In the case of a sharp V-notch, the strain energy release rate may be computed by means of the following general formula providing the SIF of a crack placed at the notch vertex and directed along the bisector [12]:

$$K_I = \mu(\omega) K_I^* a^{\lambda-1/2} \tag{5}$$

where a is the crack length (Fig. 1b). Eq. (5) is valid under the assumptions that the crack is much shorter than the notch depth and the specimen size, i.e. $a \ll e, h$ (Fig. 1). In [5], an analytical expression for the dimensionless function $\mu(\omega)$ was provided by means of weight functions available in Tada and Paris SIF handbook [24]; note that other estimates of function $\mu(\omega)$ have been recently provided in [17,18]. It is worth observing that Eq. (5) encompasses the limit cases $K_I = K_I(e)$, when the re-entrant corner becomes a crack of depth e ($\omega = 0^\circ \Rightarrow \lambda = 1/2$, $\mu = 1$, $K_I^* = K_I$), and:

$$K_I = 1.12\sigma\sqrt{\pi a} \tag{6}$$

when the notch becomes a flat edge ($\omega = 180^\circ \Rightarrow \lambda = 1$, $\mu = 1.12\sqrt{\pi}$, and $K_I^* = \sigma$). In Sections 5 and 6 the case $\omega = 120^\circ$ will be considered, for which, according to the values provided in [18], $\mu = 1.161$.

Eq. (5) together with Irwin's relationship ($G = K_I^2/E'$) provides the following expression for the strain energy release $\Delta\Phi$:

$$\Delta\Phi = \int_0^{\Delta a} \frac{K_I^2}{E'} da = \frac{(\mu K_I^*)^2}{2\lambda E'} \Delta a^{2\lambda} \tag{7}$$

where E' is the Young's modulus in plane strain elastic problems. Upon substitution of Eq. (7) into the energy balance (4) we get:

$$G = \frac{(\mu K_I^*)^2}{2\lambda E'} \Delta a^{2\lambda-1} \geqslant G_F \tag{8}$$

Since the exponent of the crack advancement Δa is always positive, Eq. (8) provides a lower bound [15] for the crack advancement. Furthermore, this lower bound decreases as the load (i.e. K_I^*) increases.

According to the coupled FFM criterion, Eq. (8) is only a necessary condition for failure to occur. The other condition that has to be fulfilled is that, prior to crack advancement, the average stress $\bar{\sigma}$ on Δa must exceed the material tensile strength σ_u. Hence, by means of Eq. (1):

$$\bar{\sigma} = \frac{1}{\Delta a} \int_0^{\Delta a} \sigma_x dy = \frac{K_I^*}{\lambda} (2\pi\Delta a)^{\lambda-1} \geqslant \sigma_u \tag{9}$$

Since the exponent of the crack advancement Δa is always negative, Eq. (9) provides an upper bound [15] for the crack advancement. Noteworthy, this upper bound increases along with the load (i.e. K_I^*). It means that for low load levels, the two conditions (8) and (9) cannot be contemporaneously satisfied, while they can for higher loads. The lowest load fulfilling Eqs. (8) and (9) provides the crack increment Δa as well as the failure load, i.e. the critical value K_{Ic}^* of the generalized SIF K_I^*:

$$K_{Ic}^* = \xi(\omega) \frac{K_{Ic}^{2(1-\lambda)}}{\sigma_u^{1-2\lambda}} \quad \text{with } \xi(\omega) = \lambda^\lambda \left[\frac{(2\pi)^{2\lambda-1}}{\mu^2/2} \right]^{1-\lambda} \tag{10}$$

Based on the values of λ and μ previously given, for $\omega = 120^\circ$ Eq. (10) yields $\xi = 1.017$. Eq. (2) together with the estimate of the generalized fracture toughness (10) provides the failure load (under mode I loading conditions) for most of V-notched components [5]. However, as observed in the Introduction, Eq. (2) provides infinite failure loads for notch depths tending to zero, since K_I^* tends to zero. This drawback should have been expected, since Eq. (5) has been derived under the assumption $a \ll e$, i.e. it does not hold true for shallow notches. In the following sections we will remove this hypothesis by performing a two-scale asymptotic analysis of the geometry involved. The asymptotic analysis will be addressed following the procedure outlined in [19], where it was exploited to analyse the blunting effect of the notch root radius in ceramic materials.

3. Perturbation theory and asymptotic matching

By decomposing a tough problem into a number of relatively easy ones, perturbation theory aims at obtaining approximate solutions to problems involving a small parameter ε.

Perturbations can be regular or singular. A basic feature of all regular perturbation problems is that the exact solution for small but nonzero ε smoothly approaches the solution of the unperturbed ($\varepsilon = 0$) problem. Referring to differential equations, a singularly perturbed differential equation is usually related to the presence of the parameter ε in front of the highest order derivative. The solutions of such equations are characterized by the presence of a boundary layer, i.e. a narrow region where the solution changes rapidly and whose thickness approaches 0 as $\varepsilon \to 0$.

If an analytical solution is not achievable, an approximate solution can be obtained by dividing the interval on which the boundary-value problem is posed into two overlapping subintervals, the inner (where the boundary layer takes place) and outer domains. The solution can be computed in each interval up to some extent: missing terms are determined by imposing

that a region must exist where the two solutions overlap. This technique is named asymptotic matching and allows one to achieve the final (approximate) solution.

As a mathematical technique, asymptotic matching has been applied in many fields. Here we will follow the formalism proposed in [15,16,19,27] by Leguillon to address fracture mechanics problems. However, several other authors used this technique to handle crack problems; to make an example for a geometry close to ours, here we cite Fieldstad et al. [10], where the asymptotic approach was exploited to determine the SIF for semi-elliptic surface shallow and deep cracks at V-notches.

In what follows, the asymptotic matching technique will be applied to study the effect of shallow notches. In such a case, the notch itself will be considered as a small perturbation of size e. As can be easily argued, the perturbation is singular since a stress intensification/concentration is present as far as $e \neq 0$, whereas it suddenly disappears as the notch vanishes ($e = 0$). It is important to emphasize that the analysis carried out in this and the following section is general, i.e. it can be applied to any notch shape (V-notches, round notches, etc.) and to any specimen geometry and load, the unique restriction being the symmetry. However, a numerical example of the proposed procedure as well as a comparison with experimental data will focus on three-point bending (TPB) specimens with (sharp) V-notches ($\omega = 120°$).

Hence, let us consider a specimen with a small notch loaded in mode I conditions, as is, for instance, the one represented in Fig. 2a. We assume that the notch depth e is small with respect to the other geometrical dimensions, i.e. the notch is shallow.

The actual displacement field is $\underline{U}^e$ (the underscore denoting vectors), where the superscript e reminds the dependence of the displacement field on the notch. Denoting by (r, θ) the polar coordinates of a system centred at the bottom of the mid-span cross section (see Fig. 2b), the actual solution can be expressed as

$$\underline{U}^e(r,\theta) = \underline{U}^0(r,\theta) + \text{small correction} \tag{11}$$

where $\underline{U}^0$ is the solution of the plain, un-notched specimen (i.e. when $e = 0$). As r tends to zero, it can be expanded as:

$$\underline{U}^0(r,\theta) = \underline{U}^0(r=0) + \sigma_n r \underline{u}(\theta) + \cdots \tag{12}$$

The first term at the right-hand side represents the irrelevant rigid translation; σ_n is the nominal stress, i.e. the normal stress that would occur at the origin if the specimen were un-notched; $\underline{u}(\theta)$ is a function of the angular coordinate θ as well as of the material elastic parameters E', ν' (not marked explicitly). Eq. (11) represents the outer field solution, since it is an approximation which breaks down in the neighbourhood of the notch.

To have a detailed description of the actual solution $\underline{U}^e$ close to the notch, the domain is stretched by $1/e$. The new dimensionless radial coordinate is $\rho = r/e$. The notch size attains a unit measure and, as $e \to 0$, the inner domain becomes unbounded (see Fig. 3a). In the inner domain the actual solution is assumed to expand as follows:

$$\underline{U}^e(r,\theta) = \underline{U}^e(e\rho,\theta) = F_0(e)\underline{V}^0(\rho,\theta) + F_1(e)\underline{V}^1(\rho,\theta) + \cdots \tag{13}$$

with $\lim_{e\to 0} F_1(e)/F_0(e) = 0$.

Boundary conditions to determine the functions $\underline{V}^i$ are needed. These conditions can be derived by the asymptotic matching, i.e. an intermediate region exists where the two expansions (the outer, Eq. (11), and the inner, Eq. (13)) hold true. In other words, expression (13) for $\rho \to \infty$ must coincide with Eq. (11) for $r \to 0$ (i.e. with Eq. (12)). This is true if:

$$F_0(e) = 1, \quad F_1(e) = \sigma_n e, \quad \underline{V}^0(\rho = 0) = \underline{U}^0(r = 0) \tag{14}$$

and

$$\underline{V}^1(\rho,\theta) = \rho \underline{u}(\theta) \quad \text{for } \rho \to \infty \tag{15}$$

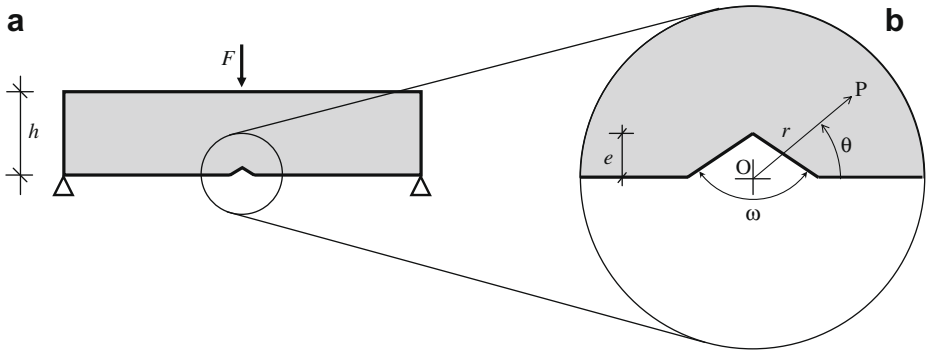

Fig. 2. Specimen with a shallow ($e << h$) notch (a) and detail of the notch vertex with the polar coordinate system (b).

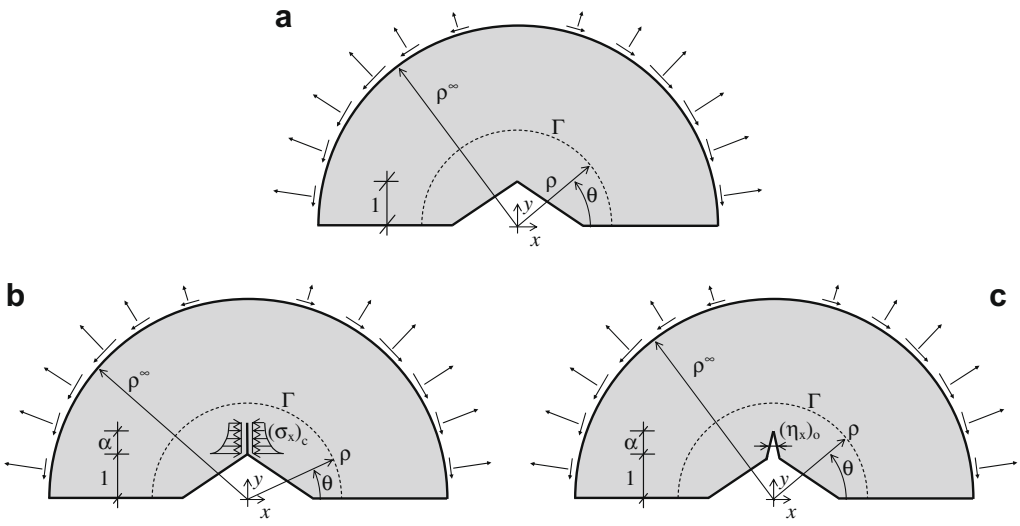

Fig. 3. Inner domain and contour integral Γ: (a) without the crack, i.e. $\alpha = 0$; (b) with the crack at the V-notch root, i.e. $\alpha \neq 0$, but with closure stresses $(\sigma_x)_c$; (c) with the open crack, $(\eta_x)_o$ being the crack opening displacement. The stress–strain fields of schemes (a) and (b) are identical.

Substituting Eq. (14) into Eq. (13), finally yields:

$$\underline{U}^e(r,\theta) = \underline{U}^e(\rho e,\theta) = \underline{U}^0(r=0) + \sigma_n e \underline{V}^1(\rho,\theta) + \cdots \tag{16}$$

In order to apply the coupled FFM criterion, we need to evaluate the displacement field when a small crack a is present at the notch root. Because of the stretched coordinate, in the inner domain the length of the crack is $\alpha = a/e$ (see Fig. 2b). We can follow the same procedure outlined before to get the following expansion:

$$\underline{U}^e(r,\theta,a) = \underline{U}^e(\rho e,\theta,\alpha e) = \underline{U}^0(r=0) + \sigma_n e \underline{V}^1(\rho,\theta,\alpha) + \cdots \tag{17}$$

Eq. (17) generalizes Eq. (16) when $\alpha \neq 0$; hence, thereafter we rewrite $\underline{U}^e(r,\theta)$ and $\underline{V}^1(\rho,\theta)$ as $\underline{U}^e(r,\theta,0)$ and $\underline{V}^1(\rho,\theta,0)$, respectively.

The great advantage of this approach [15,19] is that the displacement field $\underline{V}^1(\rho,\theta,\alpha)$ is independent of the applied load, geometry and notch size. $\underline{V}^1(\rho,\theta,\alpha)$ can be computed once for all by a finite element analysis. Since the inner domain is unbounded, we need to bound it artificially by limiting the radial coordinate at $\rho = \rho^\infty$; ρ^∞ has to be large if compared with the dimensionless notch size (i.e. unity) and crack length (i.e. α). In our numerical simulations, we assumed $\rho^\infty = 200$. For what concerns the boundary condition (15) on the ρ^∞-circumference, one can choose Dirichlet as well as Neumann conditions:

$$\underline{V}^1(\rho,\theta) = \rho \underline{u}(\theta) \quad \text{or } \sigma\left[\underline{V}^1(\rho,\theta)\right]\underline{n} = \begin{pmatrix} \cos^2\theta \\ -\cos\theta\sin\theta \end{pmatrix} \tag{18}$$

where $\sigma\left[\underline{V}^1\right]$ denotes the Cauchy stress tensor associated to the displacement field $\underline{V}^1$, and $\underline{n}$ is the normal to the boundary. In the numerical simulations, we used Neumann boundary conditions.

4. The strain energy release

The strain energy release produced by a short crack a at the notch root (Fig. 3) may be computed by a suitable application of Betti's theorem [15].

Let us consider a region surrounding the notch, e.g., for the sake of simplicity, bounded by a circumference Γ of radius r (ρ in the inner domain; see Fig. 3, dashed line). Then, consider two configurations: the former one without the crack of length a at the notch root (denoted by "c", since the crack is closed, Fig. 3a); the latter one with the crack (denoted by "o", since the crack is open, Fig. 3c). In the "open" configuration, the crack opening displacement profile is indicated by $(\eta_x)_o$. Observe that the configuration without the crack (Fig. 3a) can be seen as if the crack were initially open but with a stress distribution $(\sigma_x)_c$ acting on the crack lips and closing the crack. The geometry being now the same (Figs. 3b and 3c), we may apply Betti's theorem to the region surrounded by Γ. It states the equality of the reciprocal works. Since there are no body forces, only stresses acting at the region boundaries have to be taken into account. Hence:

$$\int_0^\pi \underline{t}_o \cdot \underline{\eta}_c r \mathrm{d}\theta = \int_0^\pi \underline{t}_c \cdot \underline{\eta}_o r \mathrm{d}\theta + \int_e^{e+a} (\sigma_x)_c \times (\eta_x)_o \mathrm{d}y \tag{19}$$

where $\underline{t}$ is the stress vector acting on the boundary, and $\underline{\eta}$ is the displacement field and a dot $(\cdot)$ represents the scalar product. Since mode *I* loading conditions have been considered, only the normal component σ_x of the stress and the horizontal displacement η_x appear in the second integral at the right-hand side (x, y being the horizontal and vertical axes, respectively). It is easily recognized that this term is twice the crack closure work (per unit thickness), i.e. the strain energy release $\Delta\Phi$ due the crack formation. Therefore:

$$\Delta\Phi = \frac{1}{2}\int_0^{\pi} (\underline{t}_o \cdot \underline{u}_c - \underline{t}_c \cdot \underline{u}_o) r \mathrm{d}\theta \tag{20}$$

Eq. (20) holds for any integration path Γ, i.e. for any line starting and ending at the notch flanks. Since the left hand side represents the strain energy release caused by the presence of the crack, it follows that the contour integral at the right-hand side is path-independent. In the present case, since the contour Γ is a circumference, the integral in Eq. (20) does not depend on its radius r. According to the notation used in the previous section, Eq. (20) may be rewritten as

$$\Delta\Phi = \frac{1}{2}\int_0^{\pi} \{\sigma[\underline{U}^e(r,\theta,a)]\underline{n} \cdot \underline{U}^e(r,\theta,0) - \sigma[\underline{U}^e(r,\theta,0)]\underline{n} \cdot \underline{U}^e(r,\theta,a)\} r \mathrm{d}\theta \tag{21}$$

Taking the integral in the inner domain, i.e. using the expansions (16) and (17), yields:

$$\Delta\Phi = \frac{\sigma_n^2}{E'} e^2 \int_0^{\pi} \frac{E'}{2} \left\{\sigma\left[\underline{V}^1(\rho,\theta,\alpha)\right]\underline{n} \cdot \underline{V}^1(\rho,\theta,0) - \sigma\left[\underline{V}^1(\rho,\theta,0)\right]\underline{n} \cdot \underline{V}^1(\rho,\theta,\alpha)\right\} \rho \mathrm{d}\theta \tag{22}$$

The contour integral at the right-hand side depends only on the dimensionless parameter α (and on the notch shape). In fact: (i) it does not depend on the material parameters E', ν' (since $\underline{V}^1 \propto 1/E'$ and a numerical check shows that the Poisson ratio has no influence); (ii) θ disappears by integration; (iii) ρ does not affect the integral since it is path-independent; (iv) the integral is independent of the size of the perturbation (i.e. the notch) and of the load thanks to the asymptotic matching technique used above. The information about the load, the material and the notch size are collected in the term $(\sigma_n e)^2/E'$ multiplying the contour integral in Eq. (22), which will be hereafter denoted by $I(\alpha)$.

5. Failure criterion for shallow V-notches

In this section we apply the asymptotic matching technique outlined in Sections 3 and 4 to the particular case of shallow V-notches with opening angle $\omega = 120°$. In Table 1, some of the computed values of the contour integral I vs. α are provided. Observe that, beyond the stress-strain field of the uncracked case, each I-value needs a proper finite element analysis providing the displacement field $\underline{V}^1(\rho,\theta,\alpha)$ and the related stresses $\sigma\left[\underline{V}^1(\rho,\theta,\alpha)\right]$, as can be evinced by the expression of the contour integral in Eq. (22). The numerical analyses were performed by means of LUSAS® finite element code.

According to Eq. (4) and Eq. (22), the strain energy release rate becomes:

$$G = \frac{\Delta\Phi}{\Delta a} = \frac{\sigma_n^2 e}{E'} g(\alpha) \tag{23}$$

where function $g(\alpha) = I(\alpha)/\alpha$ represents the dimensionless strain energy release rate; it is plotted in Fig. 4 and tabulated in Table 1 on the basis of the numerically computed values of $I(\alpha)$.

It is instructive to obtain the asymptotic expressions of $g(\alpha)$ for $\alpha \to 0$ and $\alpha \to \infty$. The former case corresponds to assuming $a << e$ ($<<h$). It is therefore a particular case of the one we dealt with in Section 2. It is even simpler, since in such a case dimensional analysis arguments provide the following expression for the generalized SIF:

$$K_I^* = \beta(\omega)\sigma_n e^{1-\lambda} \tag{24}$$

Eq. (24) may be also regarded as the formula providing the value of the generalized SIF in a semi-infinite plate under uniform remote tensile stress $\sigma = \sigma_n$ (see Fig. 5). It encompasses the limit cases $K_I = 1.12\ \sigma_n \sqrt{\pi e}$ ($\omega = 0° \Rightarrow \lambda = 1/2$, $\beta = 1.12\sqrt{\pi}$) and $\sigma = \sigma_n$ ($\omega = 180° \Rightarrow \lambda = 1$, $\beta = 1$). For intermediate cases, the values of the dimensionless coefficient β can be found, for instance, in [9], by comparing the theoretical displacement field at the notch tip with the numerical result of a finite element

Table 1
Values of the path-independent integral $I(\alpha)$, of the dimensionless stress energy release rate $g(\alpha)$ and dimensionless average normal stress $\bar{t}(\alpha)$ for different values of the crack length to notch depth ratio α.

α	$I(\alpha)$	$g(\alpha)$	$\bar{t}(\alpha)$
0	0	0	∞
0.5	2.27	4.55	2.28
1	5.74	5.74	1.79
2	15.7	7.83	1.45
4	47.3	11.8	1.24
∞	∞	∞	1

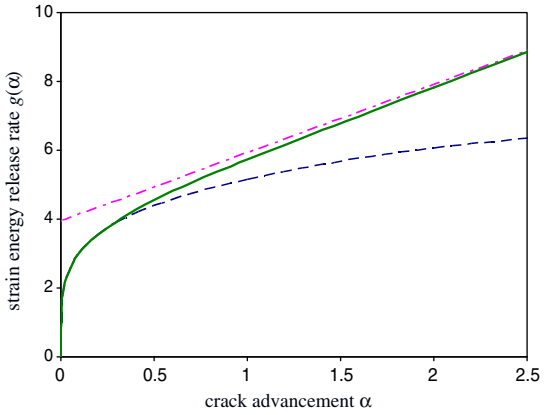

Fig. 4. Crack at the vertex of a shallow V-notch ($\omega = 120°$): dimensionless plot of the strain energy release rate vs. crack advancement (continuous line); asymptotic expansions for $\alpha \to 0$ (dashed line) and for $\alpha \to \infty$ (dash–dotted line).

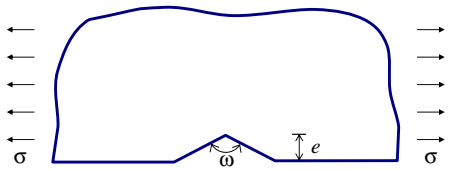

Fig. 5. Semi-infinite notched plate under uniform remote tension.

analysis. However, in the present analysis, we exploited the H-integral technique (i.e. a path-independent integral, see [23]) to get the approximate value $\beta = 2.172$ for $\omega = 120°$. Eventually, note that Eq. (24) can be seen as a limit case ($h \to \infty$) for Eq. (15) in [2], which provides the generalized SIF in a finite slab.

Upon substitution of Eq. (24) into Eq. (8) and comparison with Eq. (23), we get:

$$g(\alpha) \to \frac{\mu^2 \beta^2}{2\lambda} \alpha^{2\lambda - 1} \quad \text{as } \alpha \to 0 \tag{25}$$

Note that, although not marked explicitly, the asymptotic expression of $g(\alpha)$ depends also on the notch opening angle ω through λ, β and μ.

In the latter case, i.e. $\alpha \to \infty$, the crack advancement is much larger than the notch depth: ($h >>$) $a >> e$. In such a limit situation, the effect of the notch size and shape becomes negligible with respect to the crack advancement and the strain energy release may be evaluated simply by integrating between e and $(e + a)$ Irwin's relationship ($G = K_I^2 / E'$), where the SIF is simply given by the edge crack formula (Eq. (6)). Comparison with Eq. (23) yields:

$$g(\alpha) \to \frac{1.12^2 \pi}{2} (\alpha + 2) \quad \text{as } \alpha \to \infty \tag{26}$$

Observe that, differently from Eq. (25), the asymptotic expression (26) does not depend on ω, i.e. it holds true for any notch shape. The asymptotes (25) and (26) are plotted together with function $g(\alpha)$ in Fig. 4.

The stress requirement for crack advancement is much easier to achieve, since we only need the dimensionless average normal stress $\bar{t}(\alpha)$ in front of the vertex, over a segment of length α, in the inner domain of the closed configuration (Fig. 3b):

$$\bar{t}(\alpha) = \frac{1}{\alpha} \int_1^{1+\alpha} \sigma_x [\underline{V}^1(\rho, \theta, 0)]\big|_{\theta = \pi/2} \mathrm{d}\rho \tag{27}$$

Function $\bar{t}(\alpha)$ is plotted in Fig. 6 and tabulated in Table 1. Also in this case it is worth obtaining the two asymptotes. For $\alpha \to 0$, the asymptotic stress field (Eq. (1)) holds true, the generalized SIF being now given by Eq. (24). Therefore, the dimensionless average stress becomes:

$$\bar{t}(\alpha) \to \frac{\beta}{\lambda} (2\pi\alpha)^{\lambda - 1} \quad \text{as } \alpha \to 0 \tag{28}$$

On the other hand, for $\alpha \to \infty$, the notch effect vanishes and

$$\bar{t}(\alpha) \to 1, \quad \text{as } \alpha \to \infty \tag{29}$$

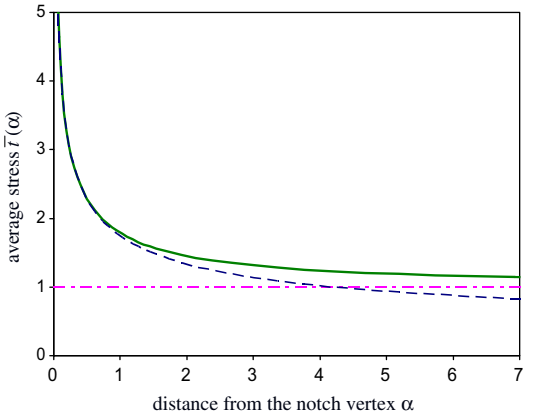

Fig. 6. Dimensionless plot of the average normal stress in front of the vertex of a shallow V-notch with $\omega = 120°$ (continuous line); asymptotic expansions for $\alpha \to 0$ (dashed line) and for $\alpha \to \infty$ (dash–dotted line).

As in the energetic analysis, the left asymptote depends on the notch opening angle ω, whereas the right one does not. The asymptotes (28) and (29) are plotted together with function $\bar{t}(\alpha)$ in Fig. 6.

We are now able to apply the coupled FFM criterion outlined in Section 2. Failure occurs if and only if:

$$G = \frac{\sigma_n^2 e}{E'} g(\alpha) \geqslant G_F \tag{30}$$

and:

$$\bar{\sigma} = \sigma_n \bar{t}(\alpha) \geqslant \sigma_u \tag{31}$$

The lowest nominal stress σ_n fulfilling Eqs. (30) and (31) provides the failure stress σ_f. Since functions $g(\alpha)$ and $\bar{t}(\alpha)$ are monotonically increasing and decreasing with α, respectively (see Figs. 4–6), Eq. (30) provides a lower bound for α, whereas Eq. (31) provides an upper bound. Consequently, failure occurs when the inequality symbols are replaced by the equality ones and the two inequalities (30) and (31) become a system of two equations in the two unknowns: the nominal stress and the crack advancement at incipient failure, σ_f and α_c, respectively. Getting σ_f from both Eqs. (30) and (31):

$$\sigma_f = \frac{K_{Ic}}{\sqrt{e g(\alpha_c)}} = \frac{\sigma_u}{\bar{t}(\alpha_c)} \tag{32}$$

By introducing the brittleness number s as proposed[1] by Carpinteri in [1]:

$$s = \frac{K_{Ic}}{\sigma_u \sqrt{e}} \tag{33}$$

Eq. (32) may be cast in the following form:

$$\frac{\sqrt{g(\alpha_c)}}{\bar{t}(\alpha_c)} = s \tag{34}$$

Eq. (34) represents an equation in α_c, the brittleness number being a known quantity providing the necessary information about the material and the geometry. Eq. (34) has to be solved numerically, since functions $g(\alpha)$ and $\bar{t}(\alpha)$ are known numerically. Once the critical crack advancement α_c is known, the nominal stress σ_f at failure may be obtained by one of the equalities in Eq. (32), e.g.:

$$\frac{\sigma_f}{\sigma_u} = [\bar{t}(\alpha_c)]^{-1} \tag{35}$$

which provides the failure stress in dimensionless form. From a physical point of view, Eq. (35) represents the strength of the notched specimen normalized with respect to the strength of the corresponding un-notched specimen. In other words, Eq. (35) provides a measure of the strength reduction caused by the presence of a notch. Obviously, the ratio (35) is always smaller than unity. Finally, observe that, once the relation between load and nominal stress is known (i.e. the outer problem is solved), σ_f provides also the failure load.

[1] Note that, with respect to the brittleness number definition given in [1], the specimen size h is here replaced by the notch depth e, since it is the only relevant geometrical length of the problem.

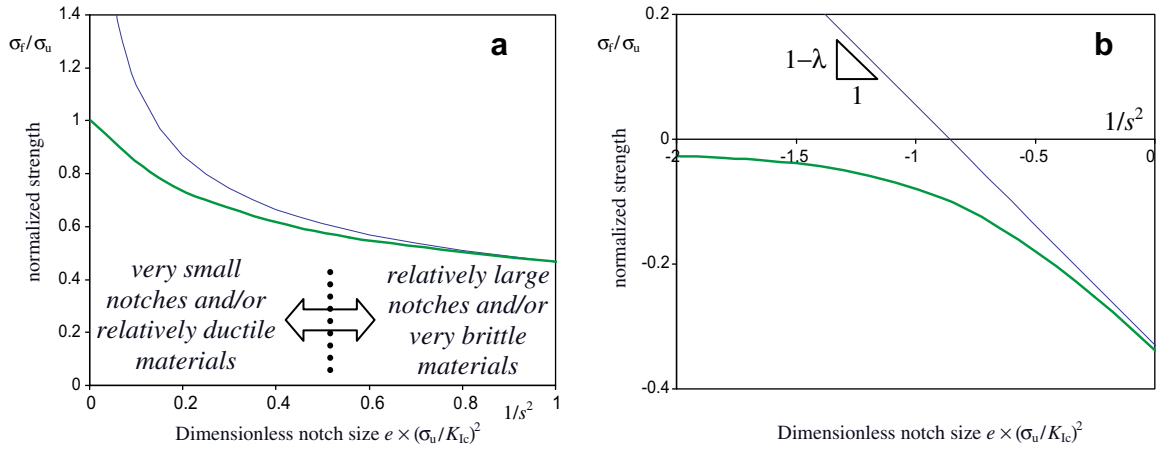

Fig. 7. Normalized strength vs. dimensionless notch size (a); bi-logarithmic plot (b). The thick line corresponds to the present model; the thin line represents the $K_I^* = K_{Ic}^*$ criterion (Eq. (36)).

Concerning the limit cases, it should be noted that, for $s \to \infty$, i.e. for very small notches and/or relatively ductile materials, the structure becomes insensitive to the notch and the nominal stress at failure coincides with the ultimate tensile strength as anticipated in [2]. This result is valid for any notch shape. On the other hand, for $s \to 0$, i.e. for relatively large notches and/or very brittle materials, the result depends on the notch shape. In the case of V-notches, when $s \to 0$, it means that failure is accurately predicted by Eq. (2), i.e. $K_I^* = K_{Ic}^*$. Substituting Eq. (10) and Eq. (24) into Eq. (2) yields:

$$\frac{\sigma_f}{\sigma_u} = \frac{\xi}{\beta} s^{2(1-\lambda)} \tag{36}$$

Summarizing, according to the present model the normalized (residual) strength of a shallow-notched component may be evaluated in three steps: (i) compute the brittleness number s, see Eq. (33); (ii) solve Eq. (34) by means of functions $g(\alpha)$ and $\bar{t}(\alpha)$ (Figs. 4–6, Table 1), thus finding the crack advancement at failure α_c; (iii) evaluate the normalized strength through Eq. (35). In Fig. 7a the normalized strength is plotted vs. $1/s^2$, i.e. the dimensionless notch size $e \times (\sigma_u/K_{Ic})^2$, together with Eq. (36). As expected, Eq. (36) provides a good approximation to the (more sophisticated) present model for $s \to 0$, whereas it yields an overestimation of the structural strength as the notch becomes smaller and smaller. In the limit of a vanishing notch ($s \to \infty$), Eq. (36) provides an infinite failure load. As stated in the Introduction, this is a shortcoming shared with LEFM and is overcome by the present approach.

In Fig. 7b, the preceding diagram is plotted in a bi-logarithmic scale. In such a case, Eq. (36) is represented by a straight line of negative slope $(1-\lambda)$: the prediction of the present model departs from this straight line for large s values. Finally, it is worth noting that Fig. 7 describes the effect of the notch size and not the size effect, since the structural size is assumed to be constant and much larger than both the notch and the crack advancement.

6. Comparison with experimental data

Since the model developed up to now is based (as LEFM) on a surface energy dissipation (Eq. (4)), it is argued that it works mainly for brittle or quasi-brittle material specimens. To check its soundness, its predictions are compared in the present section with the data obtained by a series of TPB tests (Fig. 2) on polystyrene specimens. The specimen size was 3.7 mm (thickness) × 76 mm (length) × 18 mm (height). At the mid-span, a shallow and sharp (the notch root radius was kept smaller than 10 μm) V-notch with opening angle equal to 120° was machined in each specimen. Three different notch depths e were tested, i.e. 0.2, 0.6, and 1.8 mm, thus yielding a relative notch depth e/h, respectively equal to 1/90, 1/30, 1/10. Each geometry was tested five times; all the specimens showed a linear elastic behaviour up to failure. Five un-notched specimens were also tested, providing an average value of the tensile strength σ_u equal to 70.6 MPa, whereas the fracture toughness was derived by previous tests performed on cracked specimens of the same material and stock, yielding K_{Ic} = 2.23 MPa$\sqrt{m}$. Thus the brittleness number (Eq. (33)) can be computed for each geometry and the procedure outlined in the previous section applied to get the predictions of the normalized strength. More details about experimental setup and all the recorded values of failure loads can be found in [6].

By definition, the ratio of each failure load to the average failure load of the un-notched specimens is equal to the ratio of the nominal stress at failure to the tensile strength. Comparison between theory and experiments is drawn in Fig. 8, where experimental data and theoretical predictions have been plotted vs. the relative notch depth. It is evident the excellent agreement for small notches, where the LEFM-like criterion (Eq. (2)) breaks down. On the other hand, the asymptotic approach underestimates the strength for relatively large notch depths (e.g. e/h = 1/10), but this feature had to be expected since the perturbation theory breaks down when the smallness assumption fails. However, for large notches, Eq. (2) provides

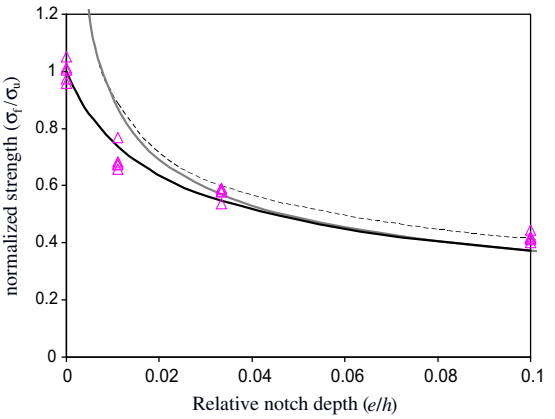

Fig. 8. Comparison between the present model and TPB tests on polystyrene specimens: experimental data, triangles; present model, black line; $K_I^* = K_{Ic}^*$ criterion using the asymptotical ($e \to 0$) value for K_I^* (Eq. (28)), gray line; $K_I^* = K_{Ic}^*$ criterion using the actual value for K_I^* (from [6]), dashed line.

excellent results if the generalized SIF is properly computed [6]. In other words, Eq. (36) never gives satisfactory results, either because it does not consider the effect of shallow notches correctly, or because the asymptotic value of the generalized SIF (24) does not hold true for notches whose size is comparable with the specimen height.

7. Conclusions

In the present paper, a multiscale analysis was developed to evaluate how the presence of a shallow V-notch affects the failure load of a brittle material specimen. The procedure outlined is applicable to any notch shape and geometry, provided that the notch is subjected to mode *I* loading conditions. Numerical results were explicitly given for specimens with a re-entrant corner of 120°. A fairly good agreement with experimental data seems to prove the soundness of the present approach in predicting the strength reduction caused by shallow V-notches. On the other hand, when applied to the same geometry, the classical criterion $K_I^* = K_{Ic}^*$ (Eq. (2)) may largely overestimate the specimen strength, as already predicted in [2]. Therefore, its use in case of shallow notches is potentially dangerous and should be avoided. The opposite occurs for deeper (i.e. full-sized) notches, when the present approach becomes inaccurate, while criterion (2) provides satisfactory results as well-known from the literature. Comparison with experimental data seems to fix the transition between shallow and full sized V-notches regimes at about 1/30–1/10 of the ligament width, at least for the TPB geometry. Note that, despite their smallness, shallow notches can significantly reduce the specimen strength (up to 50% in Fig. 8).

Acknowledgement

Authors wish to acknowledge Dr. Nardiello and Dr. Sapora for preliminary contributions to the present research developed during their Master thesis project.

References

[1] Carpinteri A. Static and energetic fracture parameters for rocks and concretes. Mater Struct 1981;14:151–62.
[2] Carpinteri A. Stress-singularity and generalized fracture toughness at the vertex of re-entrant corners. Engng Fract Mech 1987;26:143–55.
[3] Carpinteri A. Cusp catastrophe interpretation of fracture instability. J Mech Phys Solid 1989;37:567–82.
[4] Carpinteri A, Cornetti P, Barpi F, Valente S. Cohesive crack model description of ductile to brittle size-scale transition: dimensional analysis vs renormalization group theory. Engng Fract Mech 2003;70:1809–39.
[5] Carpinteri A, Cornetti P, Pugno N, Sapora A, Taylor D. A finite fracture mechanics approach to structures with sharp V-notches. Engng Fract Mech 2008;75:1736–52.
[6] Carpinteri A, Cornetti P, Pugno N, Sapora A, Taylor D. Generalized fracture toughness for specimens with re-entrant corners: experiments vs. theoretical predictions. To appear.
[7] Carpinteri A, Pugno N. Fracture instability and limit strength conditions in structures with re-entrant corners. Engng Fract Mech 2005;72:1254–67.
[8] Cornetti P, Pugno N, Carpinteri A, Taylor D. Finite fracture mechanics: a coupled stress and energy failure criterion. Engng Fract Mech 2006;73:2021–33.
[9] Dunn ML, Suwito W, Cunningham S. Stress intensities at notch singularities. Engng Fract Mech 1997;57:417–30.
[10] Fjeldstad A, Wormsen A, Härkegård G. Approximate stress intensity factors for cracked V-notched specimens based on asymptotic solutions with application to T-joints. Engng Fract Mech 2008;75:1083–98.
[11] Gómez F, Elices M. Fracture of components with V-shaped notches. Engng Fract Mech 2003;70:1913–27.
[12] Hasebe N, Iida J. A crack originating from a triangular notch on a rim of a semi-infinite plate. Engng Fract Mech 1978;10:773–82.
[13] Hebel J, Becker W. Numerical analysis of brittle crack initiation at stress concentrations in composites. Mech Adv Mater Struct 2008;15:410–20.
[14] Lazzarin P, Zambardi R. A finite-volume-energy based approach to predict the static and fatigue behavior of components with sharp V-shaped notches. Int J Fract 2001;112:275–98.
[15] Leguillon D. Strength or toughness? A criterion for crack onset at a notch. Eur J Mech A/Solid 2002;21:61–72.

[16] Leguillon D, Yosibash Z. Crack onset at a V-notch. Influence of the notch tip radius. Int J Fract 2003;122:1–21.
[17] Livieri P, Tovo R. The use of the J_V parameter in welded joints: stress analysis and fatigue assessment. Int J Fatigue 2009;31:153–63.
[18] Philipps AG, Karuppanan S, Churchman CM, Hills DA. Crack tip stress intensity factors for a crack emanating from a sharp notch. Engng Fract Mech 2008;75:5134–9.
[19] Picard D, Leguillon D, Putot C. A method to estimate the influence of the notch-root radius on the fracture toughness measurement of ceramics. J Eur Ceram Soc 2006;26:1421–7.
[20] Pugno N, Ruoff N. Quantized fracture mechanics. Philos Mag A 2004;84:2829–45.
[21] Seweryn A. Brittle fracture criterion for structures with sharp notches. Engng Fract Mech 1994;47:673–81.
[22] Sih GC, Ho JW. Sharp notch fracture strength characterized by critical energy density. Theor Appl Fract Mech 1991;16:179–214.
[23] Sinclair G, Okajima M, Griffin J. Path independent integrals for computing stress intensity factors at sharp notches in elastic plates. Int J Numer Meth Eng 1984;20:999–1008.
[24] Tada H, Paris P, Irwin G. The stress analysis of cracks. Handbook. St Louis (MO, USA): Paris Productions Incorporated; 1985.
[25] Taylor D, Cornetti P, Pugno N. The fracture mechanics of finite crack extension. Engng Fract Mech 2005;72:1021–38.
[26] Williams ML. Stress singularities resulting from various boundary conditions in angular corners of plates in extension. J Appl Mech 1952;19:526–8.
[27] Yosibash Z, Priel E, Leguillon D. A failure criterion for brittle elastic materials under mixed-mode loading. Int J Fract 2006;141:291–312.